Quantum mechanical three-dimensional wavepacket study of the O(1D)+ClH→ClO+H reaction

ARTICLE *in* JOURNAL OF MOLECULAR STRUCTURE THEOCHEM · MAY 2003

Impact Factor: 1.37 · DOI: 10.1016/S0166-1280(03)00017-4

3 AUTHORS:

Fahrettin Gogtas
Yıldırım Beyazıt Üniversitesi
24 PUBLICATIONS **100** CITATIONS
SEE PROFILE

Niyazi Bulut
Firat University
40 PUBLICATIONS **282** CITATIONS
SEE PROFILE

Sinan Akpinar
Firat University
48 PUBLICATIONS **536** CITATIONS
SEE PROFILE

ELSEVIER

Journal of Molecular Structure (Theochem) 625 (2003) 177–187

THEO CHEM

www.elsevier.com/locate/theochem

Quantum mechanical three-dimensional wavepacket study of the $O(^1D) + ClH \rightarrow ClO + H$ reaction

Fahrettin Gogtas*, Niyazi Bulut, Sinan Akpinar

Firat University, Department of Physics, 23169 Elazığ, Turkey

Received 18 November 2002; accepted 16 December 2002

Abstract

The state-to-state reaction probabilities at zero total angular momentum have been calculated for the $O(^1D) + ClH \rightarrow ClO + H$ reaction. Reaction probabilities from the ground state of ClH and going to all possible open product channels are computed over a wide range of energies. The energy dependence of the reaction probabilities shows that the reaction is strongly dominated by resonances. The product rotational and vibrational distributions are also extracted.

Keywords: Wavepacket; Resonances; State-to-state reaction probabilities

1. Introduction

The time-dependent quantum mechanical wavepacket approach has recently emerged as an important method for studying large and complex reactive scattering problems. Several time-dependent wavepacket approaches have so far been proposed for treating three-dimensional atom–diatom [1–4] and six-dimensional diatom–diatom reactive systems [5]. These studies have proved the power and potential of the quantal wavepacket method. Judson et al. [6] have discussed the problem of using time-dependent wavepackets to calculate state-to-state reaction probabilities for a full three-dimensional atom–diatom reactive scattering problem and have presented an application of their method to the $H + H_2 \rightarrow H_2 + H$ reaction. Balint-Kurti et al. [7–9] have developed a grid based time-dependent quantum method and applied it to several two-dimensional atom–diatom reactions to calculate state-to-state reaction probabilities. This method, which owes much to the earlier work of Judson et al. [6], has been extended to the full three-dimensional mathematical space needed for the exact treatment of the atom–diatom reactive scattering problem and applied to the $Li + HF(\nu,j) \rightarrow LiF(\nu',j') + H$ reaction [10]. Gray and Balint-Kurti have quite recently developed a new wavepacket method which is based on propagating only the real part of the wavepacket [11]. This new method has been tested on a few systems and comparisons have been made with experimental results or results obtained by other methods [12,13].

ClO and O reaction causes the catalyzation of ozone depletion in the stratosphere. $O(^1D) + HCl \rightarrow ClO + H$ has therefore become a popular reaction to

* Corresponding author.
E-mail address: gogtas@quantum.firat.edu.tr (F. Gogtas).

0166-1280/03/$ - see front matter © 2003 Elsevier Science B.V. All rights reserved.
doi:10.1016/S0166-1280(03)00017-4

study. It has been studied experimentally in all details [14–17]. The theoretical studies on this reaction were mainly concerned with the calculation of potential energy surface and aimed at rationalization of experimental data [18–21]. Quasiclassical trajectory calculations on model potential energy surfaces [22] and quantum mechanical wavepacket calculations on ab initio potential energy surfaces [23–26] have also been performed. However, none of these studies were able to reproduce experimental results. Quite recently Martinez et al. [27] have derived an analytical expression for the potential energy surface. This surface has been used by Valentina et al. [13] to calculate the cross sections, product state distributions and branching ratios. In another study, Valentina et al. [28] has used the method developed by Gray and Balint-Kurti [11] to calculate the state-to-state probabilities.

In this paper, we calculate the state-to-state probabilities for $O(^1D) + HCl \rightarrow ClO + H$ reaction at the $J = 0$. The main difference of this study from the earlier work done by Valentina et al. [28] is that the time-dependent Schrödinger equation is solved in an expansion in terms of the complex Chebychev polynomials and the Fourier Grid analysis is used for the extraction of the probabilities from the final wave function. The method is based on propagating whole wave function rather than the real part as it is done by Valentina et al. [28]. The paper is divided into two main sections below. In Section 2 the theory is outlined while in Section 3 the results of the computations are presented and discussed.

2. Theory

2.1. Time-dependent equations of motion

In Jacobi coordinates, there is a different set of coordinates for the reactant and product arrangement channels. Let τ be the index for these different arrangements, so that $\tau = \alpha$ indicates reactants $(O + ClH)$ and $\tau = \beta$ the products $(ClO + H)$. The total Hamiltonian operator at zero total angular momentum $(\mathbf{J} = 0)$ for any of these two arrangements in a body-fixed frame where the z axis is parallel to $\mathbf{R}_\tau$ and diatom is in the (x, z) plane may be expressed as

$$\hat{H} = -\frac{\hbar^2}{2\mu_\tau}\frac{\partial^2}{\partial R_\tau^2} - \frac{\hbar^2}{2\mu'_\tau}\frac{\partial^2}{\partial r_\tau^2} + \frac{\hbar^2}{2} \times\left(\frac{1}{\mu_\tau R_\tau^2} + \frac{1}{\mu'_\tau r_\tau^2}\right)\mathbf{j}_\tau^2 + V(\mathbf{R}_\tau, r_\tau, \gamma_\tau) \quad (1)$$

where $\mathbf{R}_\tau$ is the vector from the diatom centre-of-mass to the atom, r_τ is the diatomic internuclear vector, and γ_τ is the angle between the two vectors. $\mathbf{j}_\tau$ is the rotor angular momentum of the diatom, μ'_τ and μ_τ are the reduced masses. As proposed by Tal-Ezer and Kosloff [29] the solution of the time-dependent Schrödinger equation is written in the form:

$$\psi(R,r,\gamma,t) = \exp\left(\frac{-i\hat{H}t}{\hbar}\right)\psi(R,r,\gamma,t=0) = e^{-i/\hbar(\Delta E/2 + V_{\min})t}\sum_{n=0}^{N} J_n\left(\frac{\Delta E t}{2\hbar}\right)P_n(-i\hat{H}_{\text{norm}}) \times\psi(R,r,\gamma,t=0) \quad (2)$$

where $\psi(R,r,\gamma,t=0)$ is the initial wavefunction, $P_n(x)$ are complex Chebychev polynomials, $J_n(x)$ the Bessel functions and ΔE is the magnitude of the entire energy spread of the spectrum of the unnormalised Hamiltonian operator $\hat{H}_{\text{norm}}$. The three-dimensional form of the initial wavepacket may be on the grid written as:

$$\psi(R_\alpha, r_\alpha, \gamma_\alpha, 0) = \chi(R_\alpha)\phi_{vj}(r_\alpha)\hat{P}_j(\gamma) \quad (3)$$

where v and j are the initial vibrational and rotational quantum numbers, respectively. In Eq. (3), $\chi(R_\alpha), \phi_{vj}(r_\alpha)$ and $\hat{P}_j(\gamma)$ are the translational, vibrational and rotational components of the initial wavepacket, respectively. The vibrational eigenfunctions of the asymptotic diatomic Hamiltonian are calculated by solving the time-independent Schrödinger equation for diatomic molecule [30]. The rotational component of the wavepacket is taken as normalised associated Legendre functions. The initial wavepacket is defined in terms of the Jacobi coordinates of the reactant arrangement channel. In this work we wish to compute state-to-state reaction probabilities and must therefore follow the development of the wavepacket out into the product region. For this reason, the wavepacket is analyzed as it passes a line in the asymptotic region of the exit channel [9,10]. This necessitates

a change of the grid at some stage of the calculation, i.e. the grid must be changed from a reactant to a product grid. Clearly it is computationally advantageous to minimise the size of both the reactant and product grids, and this can only be achieved if the wavepacket is spatially localised at the time when it is transposed from one grid to the other. The initial wavepacket must therefore be chosen carefully so as to ensure that when it reaches the strong interaction region it will be highly localised. It has been proved previously that a translational wave function of the form

$$\chi(R)=\exp\left(-i\left[k_0R-\frac{k_0^2\beta}{4\sigma}\right]\right)\frac{\exp\left(\frac{i\,atan\,\beta}{2}\right)}{(1+\beta)^{1/2}}\times\exp\left(-\frac{(1+i\beta)\sigma}{(1+\beta^2)}\left[\frac{k_0\beta}{2\sigma}-(R-R_C)\right]^2\right) \quad (4)$$

gives a compact wave function as it is propagated from a point selected in the asymptotic reactant region ($R_{\alpha,\infty}$) to a point in the strong interaction region (R_C) [10].

2.2. Evaluation of the Hamiltonian operation

As seen from Eq. (2) the expansion requires repeated operation of the Hamiltonian on the initial wavefunction. A grid based method is used in the current work so that uniform grids are used for the coordinates R and r. The angular grid points correspond to Gauss–Legendre quadrature points [31,32]. The grid representation of the wavepacket associated with the point R_i, r_l, γ_n is given by:

$$\Phi_{iln}=\Phi(R_i,r_l,\gamma_n,t=0)\}=\psi(R_i,r_l,\gamma_n,t=0)\omega_n^{1/2} \quad (5)$$

where ω_n are the weights in the Gauss–Legendre quadrature formula. The action of the Hamiltonian on the wavefunction will be accomplished in the following way: since the potential energy is diagonal in co-ordinate space, its action on the wavefunction involves just the multiplication of the values of potential with those of wavefunction at the same spatial grid points.

$$[V\Phi]_{iln}=\{V(R_i,r_l,\gamma_n)\Phi_{iln}\} \quad (6)$$

The radial and angular kinetic energy operators are differential operators in co-ordinate space. The radial kinetic energy operator is, however, diagonal in momentum space [33]. For this reason, the wavefunction is transformed to its momentum representation via the Fast Fourier transform technique, multiplied by the kinetic energy at the each momentum grid point and transformed back to the co-ordinate representation.

$$\frac{\hbar^2}{2\mu_\tau}\frac{\partial^2}{\partial R_\tau^2}\Phi_{iln}=\frac{\hbar^2}{2\mu_\tau}\frac{1}{\sqrt{2\pi}}\sum_{i=1}^{N_R}e^{ik_iR_i}\times\left[k_i^2\frac{1}{\sqrt{2\pi}}\sum_{i=1}^{N_R}e^{-ik_lR_i}\Phi_{iln}\Delta R\right]\Delta k_R \quad (7)$$

and

$$\frac{\hbar^2}{2\mu'_\tau}\frac{\partial^2}{\partial r_\tau^2}\Phi_{iln}=\frac{\hbar^2}{2\mu'_\tau}\frac{1}{\sqrt{2\pi}}\sum_{l=1}^{N_r}e^{ik_lr_l}\times\left[k_l^2\frac{1}{\sqrt{2\pi}}\sum_{l=1}^{N_r}e^{-ik_lr_l}\Phi_{iln}\Delta r\right]\Delta k_r \quad (8)$$

The eigenfunctions of the angular kinetic energy operator are known to be the associated Legendre functions in the general case. The Discrete Variable representation (DVR) method allows one to define a transformation matrix which can be used to transform the wavefunction from the grid (or DVR) representation, in which a value is associated with each grid point $\{\gamma_k, k=1,2,\ldots\}$, to a fixed basis representation (FBR) corresponding to an expansion of the wavepacket in terms of normalised Legendre polynomials $\hat{P}_j(\cos\gamma_k)$. The action of the angular part of the kinetic energy operator on the wavefunction may be easily evaluated when the wavefunction is expressed as an expansion in Legendre polynomials. This requires the transformation of the wavefunction from the grid to the FBR representation. The transformation is accomplished by a unitary transformation matrix **A** defined in terms of normalised Legendre polynomials.

$$A_{j,n}=\omega_n^{1/2}\hat{P}_j(\cos\gamma_n) \quad (9)$$

if an N_γ Gauss–Legendre quadrature scheme is used then the maximum value of j in the associated FBR is $j_{max}=(N_\gamma-1)$. In the FBR representation the action of the angular part of the kinetic energy operator on

the wavefunction is accomplished by simply multiplying by $j(j+1)/2I$. The final DVR wavefunction is then obtained by carrying out an inverse transformation from the FBR to the grid or DVR representation. This inverse transformation is carried out by using the Hermitian conjugate of the matrix **A** in Eq. (9). In practice, this is all done in one step as [10]:

$$\left[\frac{\hbar^2}{2I}\mathbf{j}^2\Phi\right]_{iln'} = \sum_{n,j}\left\{A^{+}_{n',j}\frac{j(j+1)}{2I}A_{j,n}\Phi_{iln}\right\} = \sum_{n}\left\{\sum_{j}A^{+}_{n',j}\frac{j(j+1)}{2I}A_{j,n}\right\}\Phi_{iln} \quad (10)$$

where $I = ((1/\mu_\tau R_\tau^2) + (1/\mu_\tau' r_\tau^2))^{-1}$.

Thus, the action of the full Hamiltonian on the wavefunction is given by accomplishing four separate operations just discussed (i.e. Eqs. (6)–(8) and (10)). Eq. (2) is evaluated for each time step and propagation is carried on until the wavefunction has completely left the interaction region.

In general, if the minimum value of one (or both) of the length vectors is small (and this is in practice needed) and j is quite large, the angular kinetic energy, $T(\gamma) = j(j+1)/2I$ will have very large components. Such large values of the kinetic energy are unphysical and the correct wavefunction does not contain any components corresponding to them. On the other hand, such large kinetic energy components lead to an enormous number of terms to be used in the Chebychev expansion. Therefore, It is essential to eliminate these large kinetic energy terms so as to limit the length of the Chebychev expansion. The high angular kinetic energy components are therefore truncated above a reasonable value. A sharp cut-off in the kinetic energy will cause discontinuities in the momentum space representation of the wavefunction or in its derivatives, which will in turn give rise to unphysical oscillatory behavior in the spatial representation of the wavefunction. In this study, we have gradually truncated the angular kinetic energy as it becomes greater than a preassigned value [10].

2.3. Transformation of the wavepacket to product grid

A basic difficulty in the theory of reactive collisions is that the co-ordinates appropriate for reactant and product arrangements differ from each other. Several different solutions to this problem have now been developed [6,34,35]. In the present work the initial wavepacket is defined and initially propagated on a grid defined in terms of the reactant Jacobi co-ordinates. When the wavepacket has entered the interaction region it is transformed to a grid defined in terms of product Jacobi co-ordinates so that propagation into the asymptotic region of the exit channel and the final state analysis may be conveniently carried out. The advantage of this approach is that only a single coordinate, the scattering coordinate R_τ need take on large values in either grid. To use this approach, however, the wavepacket must be compact when it arrives in the strong interaction regions.

The total wavefunction must have a unique value at any given point in space. Thus if the reactant coordinates $R_\alpha, r_\alpha, \gamma_\alpha, \theta_\alpha, \phi_\alpha, \delta_\alpha$ specify the same point in space as the product coordinates $R_\beta, r_\beta, \gamma_\beta, \theta_\beta, \phi_\beta, \delta_\beta$, then:

$$\Psi(R_\alpha, r_\alpha, \gamma_\alpha, \theta_\alpha, \phi_\alpha, \delta_\alpha) = \Psi(R_\beta, r_\beta, \gamma_\beta, \theta_\beta, \phi_\beta, \delta_\beta) \quad (11)$$

The notation $\hat{R}_\alpha, \hat{r}_\alpha, \hat{\gamma}_\alpha$ is introduced to denote the values of the reactant coordinates which specify the same point in space as the product coordinates $R_\beta, r_\beta, \gamma_\beta$. Hence, the body-fixed wavefunction in the β arrangement may be written in terms of the α arrangement body-fixed wavefunction as [10]:

$$\psi(R_\beta, r_\beta, \gamma_\beta, t) = \left[\frac{R_\beta r_\beta}{\hat{R}_\alpha \hat{r}_\alpha}\psi(\hat{R}_\alpha, \hat{r}_\alpha, \hat{\gamma}_\alpha, t)\right]_{(\hat{R}_\alpha, \hat{r}_\alpha, \hat{\gamma}_\alpha) = (R_\beta, r_\beta, \gamma_\beta)} \quad (12)$$

The grid wavefunction in the β arrangement may be written as:

$$\Phi(R^i_\beta, r^l_\beta, \gamma^k_\beta, t) = \left[\frac{R_\beta r_\beta}{\hat{R}_\alpha \hat{r}_\alpha}(\omega^\beta_k)^{1/2} \times \sum_j \hat{P}_j(\hat{\gamma}_\alpha)\xi_j(\hat{R}_\alpha, \hat{r}_\alpha, t)\right]_{(\hat{R}_\alpha, \hat{r}_\alpha, \hat{\gamma}_\alpha) = (R^i_\beta, r^l_\beta, \gamma^k_\beta)} \quad (13)$$

where the expansion coefficients are evaluated using the formula:

$$\xi_j(R_\alpha, r_\alpha, t) = \sum_n \Phi(R_\alpha, r_\alpha, \gamma^n_\alpha, t)\hat{P}_j(\gamma^n_\alpha)(\omega^\alpha_n)^{1/2} \quad (14)$$

Note that in the above we have assumed that the total angular momentum is zero and that consequently all projections of the total angular momentum are also zero. The notation γ_α^n indicates the value of γ_α at the nth grid point.

Eq. (13) requires an accurate algorithm to evaluate $\xi_j(\hat{R}_\alpha, \hat{r}_\alpha, t)$ at the grid points defined in terms of the product coordinates $(R_\beta, r_\beta, \gamma_\beta.)$ The product and reactant coordinate grid points are different and a Fourier interpolation procedure is used to calculate the required values of $\xi_j(\hat{R}_\alpha, \hat{r}_\alpha, t)$ at the product grid positions from the known values of $\xi_j(R_\alpha, r_\alpha, t)$ at the reactant grid points. The interpolation of the wavefunction must be carried out accurately so as to avoid loss of flux and artificial distortions resulting from the transformation process.

2.4. Calculation of the reaction probabilities

In order to extract the other observable quantities from the wavepacket dynamics, the wavepacket must be properly analysed. This is done using techniques previously described [7]. The body-fixed wavefunction in the asymptotic region of exit channel may be expressed in terms of normalised Legendre polynomials as:

$$\psi(R_\beta, r_\beta, \gamma_\beta, t) = \sum_{j'} \xi_{j'}(R_\beta, r_\beta, t)\hat{P}_{j'}(\gamma_\beta) \tag{15}$$

The expansion coefficients may be written in terms of the grid representation of the wavefunction as:

$$\xi_{j'}(R_\beta, r_\beta, t) = \sum_{n'} \Phi(R_\beta, r_\beta, \gamma_\beta^{n'}, t)\hat{P}_{j'}(\gamma_\beta^{n'})(\omega_{n'}^\beta)^{1/2} \tag{16}$$

These expansion coefficients are analysed by taking cuts through them at a fixed (large) value of the product scattering co-ordinate $R_\beta = R_{\beta\infty}$ at each time step. A time-dependent coefficient for each final quantum state is then calculated as

$$C_{\nu' j'}(R_{\beta\infty}, t) = \int_{r_\beta=0}^{\infty} \xi_{j'}(R_{\beta\infty}, r_\beta, t)\phi_{\nu' j'}(r_\beta)\mathrm{d}r_\beta \tag{17}$$

The S matrix elements and the reaction probabilities are obtained from the Fourier transform over the time of the time-dependent coefficients $C_{\nu' j'}(R_{\beta\infty}, t)$. This Fourier transform yields the energy dependent amplitudes:

$$A_{\nu' j'}(R_{\beta\infty}, E) = \frac{1}{2\pi}\int_{t=0}^{\infty} \mathrm{e}^{iEt/\hbar} C_{\nu' j'}(R_{\beta\infty}, t)\mathrm{d}t \tag{18}$$

The (partial) reaction probabilities for the production of specific final vibrational-rotational states from a specified initial reactant level are given by [7]:

$$P_{j\nu\to\nu' j'}(E) = \left|S_{j\nu,\nu' j'}\right|^2 = \frac{\hbar^2}{\mu_\alpha\mu_\beta} k_{\nu' j'} k_{j\nu} \left|\frac{A_{\nu' j'}(E)}{f(k)}\right|^2 \tag{19}$$

where $f(k)$ is the Fourier transform of the initial translational wavepacket, E the total energy and $k_{j\nu}$, and $k_{\nu' j'}$ are the wavevectors in reactant and product regions, respectively.

3. Results and discussion

We present here the 3D quantum mechanical results of $O(^1D) + ClH \rightarrow ClO + H$ reaction for total angular momentum $J = 0$. We employed the potential energy surface of Laganà et al. [27]. Fig. 1 shows three-dimensional and contour plots of the strong interaction region of the potential energy surface as a function of O–ClH (R_α) and Cl–H (r_α) separations with the angle between the two vectors (Jacobi angle) fixed at the 120°. The figure shows clearly the existence of a well and a barrier along the reaction pathway at this angle. The co-ordinate grid used for the entrance channel propagation covers O–ClH separations of 0.62–25.78 a_o and ClH separations of 0.38–7.64 a_o 256 and 64 evenly spaced grid points were used in the R_α and r_α coordinates, respectively. In the reactant channel, the maximum value of the rotational quantum number used in the expansion of the wavefunction (designated j_{max}) was set equal to 50, which allows for several closed channels at the highest energies in the wavepacket.

The initial wavepacket was centered around a O–ClH separation of 8.63 a_o and given a kinetic energy of 0.272 eV along the entrance valley. The wavepacket had an effective range of total energy range 0.382–0.546 eV. This corresponds to that spanned by the central section of the wavepacket excluding the high and low energy tails where the probability is less than 10% of the peak value.

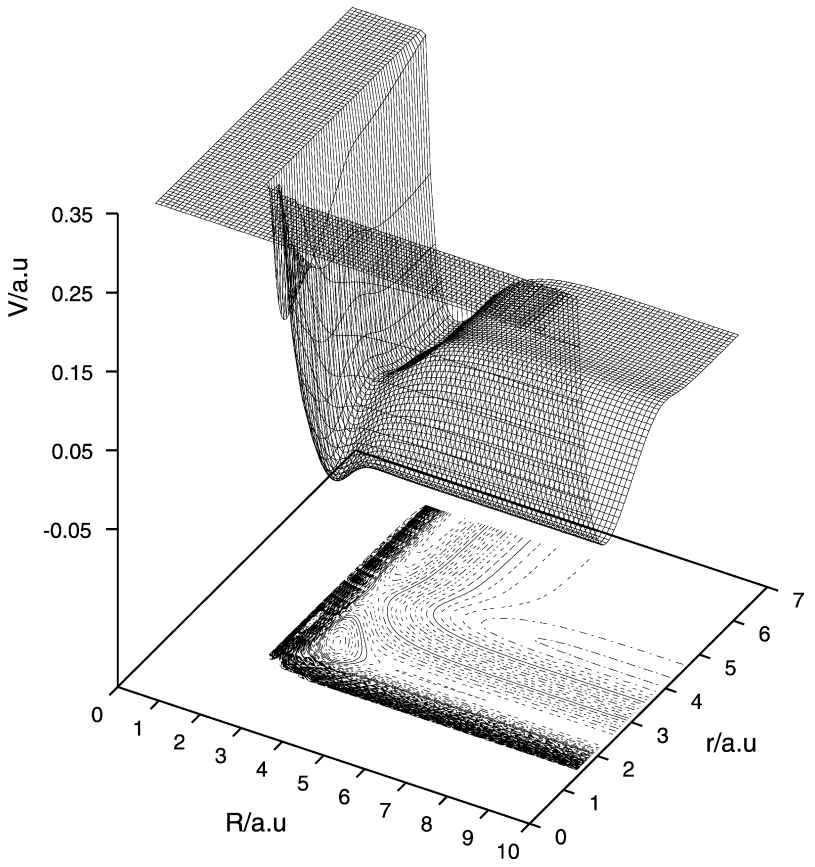

Fig. 1. Potential energy surface as a function of O–ClH (R_α) and Cl–H (r_α) separations with the Jacobi angle (γ_α) fixed at 120°.

The time step used for the propagation was approximately 2.3 fs. The wavepacket was propagated along the reactant channel first in the reactant Jacobi co-ordinates. A switching plane was defined to lie perpendicularly across the exit channel at a fixed ClH separation of 4.14 a_o. At each time step, the amplitude of the wavefunction at this plane was calculated. When this amplitude exceeds some predetermined limit (typically 1×10^{-8}) it was assumed that the head of the wavepacket had penetrated the exit channel and the wavepacket is transformed from the reactant to the product grid. The product grid was defined in such a way that only 2×10^{-7}% of the norm of the total wavepacket was not common to both grids. Clearly it is important that the region of overlap of the two grids should be sufficiently large that no significant amount of flux is lost in the transformation process. An additional numerical error inevitably arises from the interpolation process. The norm of the wavepacket on the reactant grid was 0.99999999051412, while after transformation it was 0.9999999834256141 on the product grid computed in terms of product Jacobi co-ordinates. This means that amplitude amounting to only 1×10^{-7} was lost during the process of grid switching.

The co-ordinate grid used to perform the part of the propagation in product Jacobi co-ordinates covers ClO–H separations 0.049–14.02 a_o and ClO separations 0.47–11.56 a_o. The number of grid points used to perform the propagation on the product grid was ($N_{R_\beta} = 180, N_{r_\beta} = 162$). The maximum value of the rotational quantum number used in the expansion of the wavefunction in the final rotational basis set was set equal to 100, which allows for the inclusion of several asymptotically closed channels for the range of the energies studied in the present work.

An analysis plane is located at an ClO–H separation of 11.47 a_o. This plane is defined to lie perpendicularly across the exit valley in its asymptotic region. At each time step, a cut is taken through the wavepacket along this plane and the resulting two-dimensional wavefunction is analysed into its fragment state contribution. The analysis of the wavepacket as it passes the analysis plane yields the time-dependent coefficients. The propagation is continued until all wavepacket has completely left the interaction region, in which case the time-dependent coefficients decrease to zero. The total propagation time required for the wavefunction to leave the interaction region was approximately 100,000 a.u. (2248 fs). The Fourier transform of these coefficients over the time yields the reaction probabilities. The portions of the wavepacket reflected back into the entrance channel or moving through the exit channel will eventually reach the edge of the numerical grid. If no special precautions are taken, the parts of the wavepacket that reach the edge of grid will be unphysically reflected back onto the grid, invalidating the results of calculations. In order to avoid such a reflection a complex absorbing potential with a quadratic form is employed at both edges of the grid [36,37].

The reaction probabilities for $O + ClH(\nu = 0, j = 0) \rightarrow ClO(\nu', j') + H$ covering a total energy range of 0.382–0.546 eV are shown in Figs. 2–7. All the reaction probabilities arising from this initially specified quantum state of ClH, but producing all

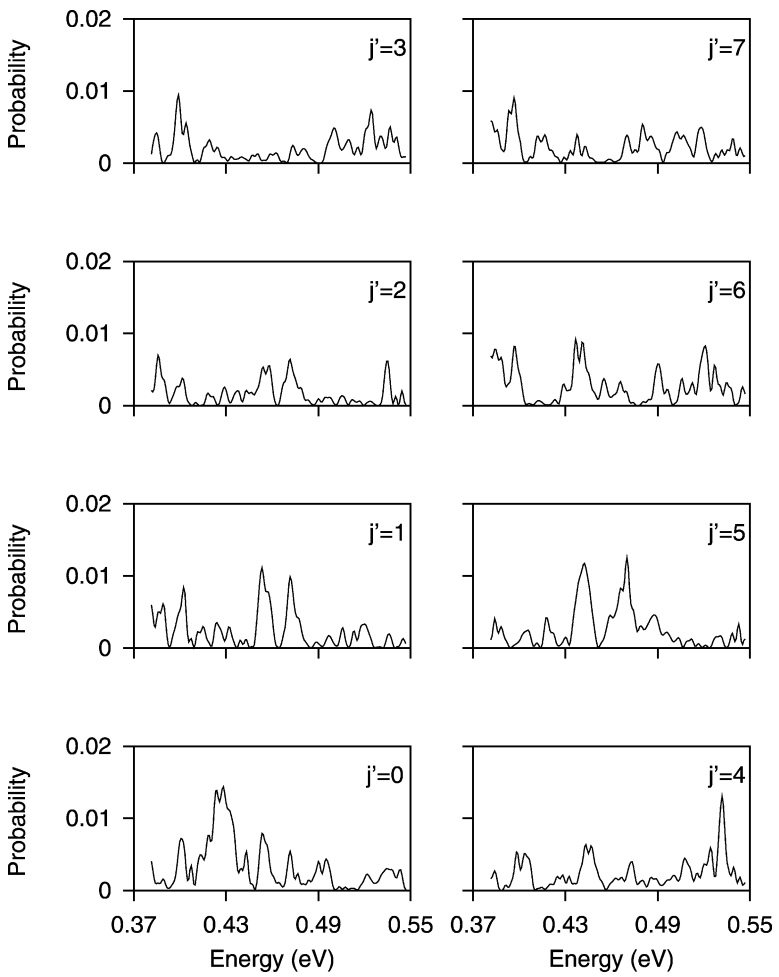

Fig. 2. Reaction probabilities for $O + ClH(\nu = 0, j = 0) \rightarrow ClO(\nu' = 0, j') + H$ reaction for $j' = 0, 1, 2, \ldots 7$ as a function of total energy.

possible final states, are obtained from a single solution of the time-dependent Schrödinger equation. The energy range is determined by the initial wavepacket and in the present case is not low enough to observe the threshold region. In order to compute reaction probabilities at lower total energies one has to start with an appropriately wavepacket which contains lower kinetic energies. In our grid-based time-dependent quantum method a longer entrance channel grid would have to be used to perform the computations at these lower kinetic energy.

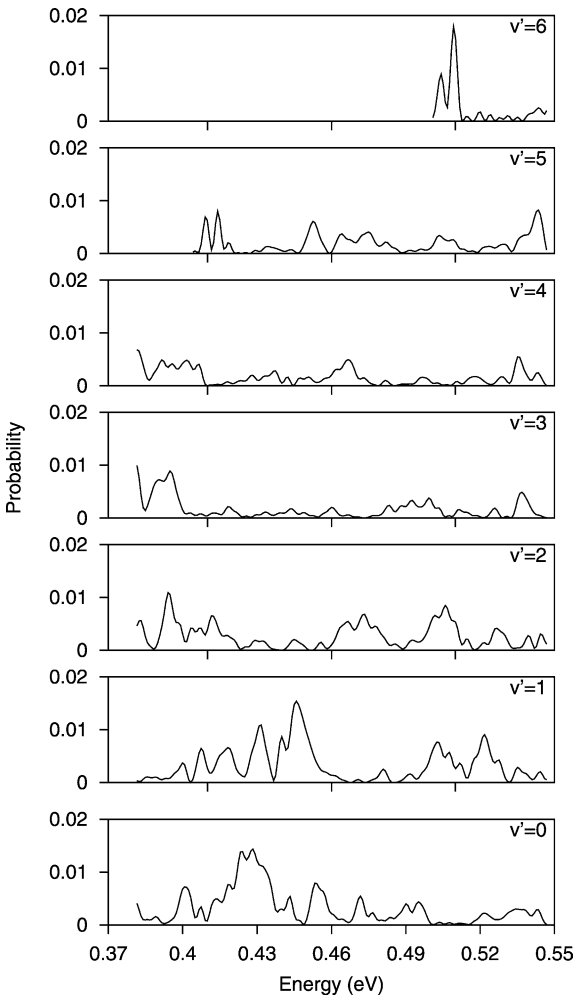

Fig. 3. Reaction probabilities for $O + ClH(\nu = 0, j = 0) \rightarrow ClO(\nu', j' = 0) + H$ reaction for $\nu' = 0, 1, 2, \ldots 6$ as a function of total energy.

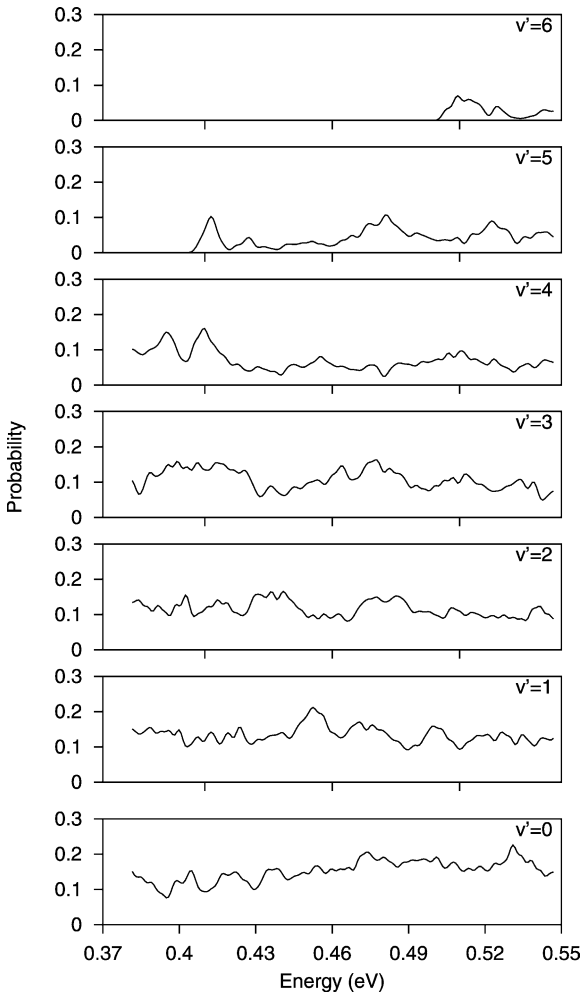

Fig. 4. Reaction probabilities for $O + ClH(\nu = 0, j = 0) \rightarrow ClO(\nu') + H$ reaction for $\nu' = 0, 1, 2, \ldots 6$ summed over all product rotational states plotted as a function of total energy.

Fig. 2 shows the state-to-state reaction probability for the reaction $O + ClH(\nu = 0, j = 0) \rightarrow ClO(\nu' = 0, j') + H$ for different product rotational states over the translational energy range contained within the initial wavepacket. The reaction probability vs translational energy plots all display many sharp resonances and most of these individual resonance features appear in all panels (each corresponding to a different product rotational state).

Fig. 3 shows reaction probabilities for transitions from the initial quantum state of the ClH reactant $(\nu = 0; j = 0)$ to various vibrational states of the ClO products $(\nu', j' = 0)$ for $\nu' = 0, 1, 2, \ldots 6$.

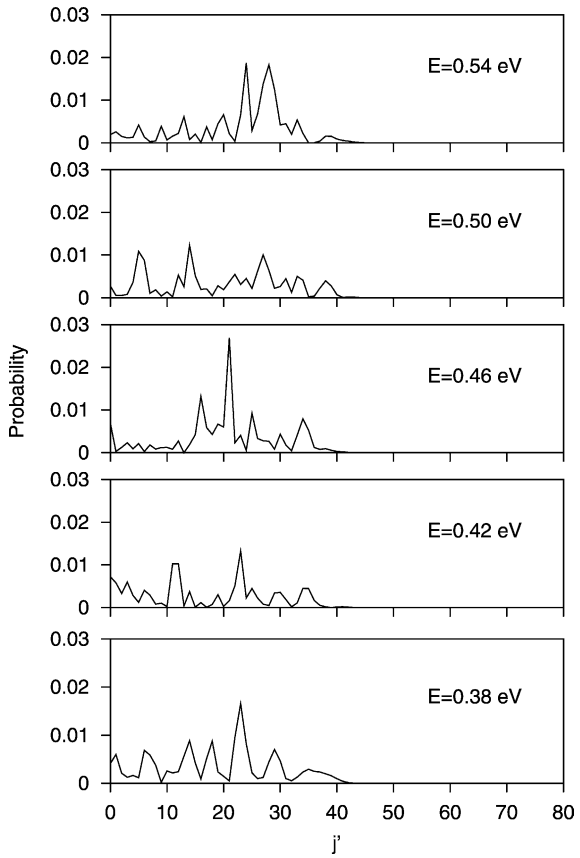

Fig. 5. Product rotational distributions for the $O + ClH(\nu = 0, j = 0) \rightarrow ClO(\nu' = 0, j') + H$ reaction plotted against j' at different total energy values. The total energy values are given in the panels.

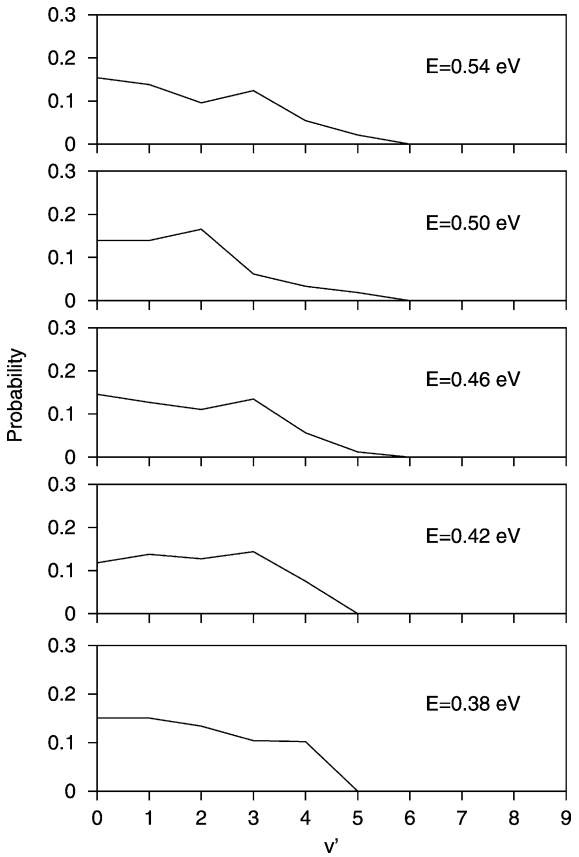

Fig. 6. Product vibrational distributions for the $O + ClH(\nu = 0, j = 0) \rightarrow ClO(\nu') + H$ reaction plotted against ν' at different total energy values. The reaction probabilities have been summed over all final rotational states j'. The total energy values are given in the panels.

As it is seen from the panels of the figure that the probability to produce vibrationally excited ClO product decreases with increasing ν' and there is a very low fraction of the probability for the $\nu' = 5$ and 6 states.

The reaction probabilities from ClH in its ground state to different product vibrational states and summed over all final rotational states are displayed in Fig. 4. The summation over all the product rotational states has largely destroyed the sharp oscillations of the reaction probability, but has not eliminated some of the broad oscillations. As it may be seen from Fig. 4, the reactions to lowest five final vibrational states show exoergic behavior in the studied energy range while those to $\nu' = 5$ and 6 states show threshold behavior.

The final state distributions at the fixed energies can also be of great utility in understanding this reaction. The product rotational distributions for the ClH reactant initially in its ground state are shown in Fig. 5 for five different total energy values (0.38, 0.42, 0.46, 0.50 and 0.54 eV). These distributions show a structured shape with no clear tendency for even-odd alternation. It may also be noticed that as the energy increased the highest peek moves to a higher j' value and also its size increases. That is the reaction produces favorably rotational excited ClO product, but the detailed results are sensitive to the energy value. Fig. 6 shows the product vibrational distributions summed over all j' for five

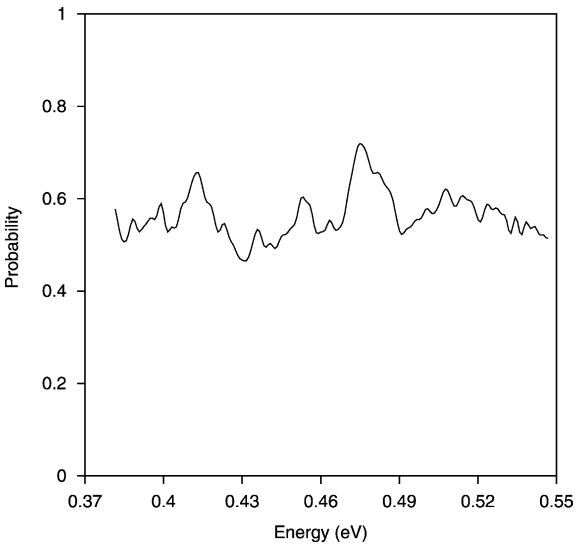

Fig. 7. Reaction probabilities for $O + ClH(\nu = 0, j = 0) + H$ reaction summed over all product vibrational and rotational states plotted as a function of total energy.

different total energy values (0.38, 0.42, 0.46, 0.50 and 0.54 eV). As may be seen from the figure, an increase in the energy does not sensitively lead to the spreading of the distribution to higher ν' values.

Fig. 7 shows the reaction probabilities summed over all final states for the reaction corresponding to the ClH reactant initially in its lowest vibrational-rotational state in the energy range of 0.382–0.546 eV. Almost all of the broad oscillations are persist showing that the reaction is strongly dominated by resonances. The same results as with Fig. 7 has also been presented in a previous study based on the propagating the real part of the wavepacket [13] for a broad energy range. As Fig. 7 is compared to Fig. 1 of that previous study, the results are in very good agreement. However, the resolution of the energy here is much sensitive to see some extra peaks.

Acknowledgements

We are grateful to Prof. Gabriel G. Balint-Kurti, Prof. Antonio Laganà and Dr Valentina Piermarini for several useful discussions. This work is supported by Scientific and Technical Research Council of the Turkish Republic (TÜBîTAK) under grand number TBAG-1739.

References

[1] D. Neuhauser, M. Baer, R.S. Judson, D.J. Kouri, J. Chem. Phys. 93 (1990) 312.
[2] D. Neuhauser, M. Baer, R.S. Judson, D.J. Kouri, Chem. Phys. Lett. 169 (1990) 372.
[3] D. Neuhauser, M. Baer, R.S. Judson, D.J. Kouri, Comput. Phys. Commun. 63 (1991) 460.
[4] D.H. Zhang, J.Z.H. Zhang, J. Chem. Phys. 101 (1994) 3671.
[5] D.H. Zhang, J.Z.H. Zhang, J. Chem. Phys. 101 (1994) 1146.
[6] R.S. Judson, D.J. Kouri, D. Neuhauser, M. Baer, Phys. Rev. A 42 (1990) 351.
[7] G.G. Balint-Kurti, R.N. Dixon, C.C. Marston, Int. Rev. Phys. Chem. 11 (1992) 317.
[8] C.C. Marston, G.G. Balint-Kurti, R.N. Dixon, Theor. Chim. Acta 79 (1991) 313.
[9] G.G. Balint-Kurti, F. Göğtas, S.P. Mort, A.R. Offer, A. Laganà, O. Garvasi, J. Chem. Phys. 99 (1993) 9567.
[10] F. Göğtas, G.G. Balint-Kurti, A.R. Offer, J. Chem. Phys. 104 (1996) 7927.
[11] S.K. Gray, G.G. Balint-Kurti, J. Chem. Phys. 108 (1998) 950.
[12] A.J.H.M. Meijer, E.M. Goldfield, S.K. Gray, G.G. Balint-Kurti, Chem. Phys. Lett. 293 (1998) 270.
[13] V. Piermarini, G.G. Balint-Kurti, S.K. Gray, F. Göğtas, A. Laganà, M.L. Harnandez, J. Phys. Chem. A 105 (2001) 5743.
[14] M.J. Molina, F.S. Rowland, Nature 249 (1974) 810.
[15] N. Basco, R.G. Norrish, Proc. R. Soc. A260 (1961) 293.
[16] N. Balucani, L. Beneventi, P. Casavecchia, G.G. Volpi, Chem. Phys. Lett. 180 (1991) 30.
[17] P.H. Wine, J.R. Wells, A.R. Ravishankara, J. Chem. Phys. 84 (1986) 1349.
[18] S. Nambu, K. Nakata, S. Iwata, Chem. Phys. 135 (1989) 75.
[19] K. Nakata, S. Iwata, J. Chem. Phys. Lett. 96 (1992) 2103.
[20] A.R. Offer, G.G. Balint-Kurti, Chem. Phys. Lett. 228 (1994) 200.
[21] A. Laganà, G. Ochoa de Aspuru, E. Garcia, J. Phys. Chem. (1995) 5.
[22] R. Schinke, J. Chem. Phys. 80 (1984) 5510.
[23] K.M. Christoffel, Y. Kim, S. Skokov, J.M. Bowman, S.K. Gray, Chem. Phys. Lett. 315 (1999) 275.
[24] M. Bittererova, J.M. Bowman, J. Chem. Phys. 113 (2000) 1.
[25] S.Y. Lin, K.L. Han, J.Z.H. Zhang, Phys. Chem. Chem. Phys. 2 (2000) 2529.
[26] S.Y. Lin, K.L. Han, J.Z.H. Zhang, Chem. Phys. Lett. 324 (2000) 122.
[27] T. Martinez, M.L. Hernandez, J.M. Alvarino, A. Laganà, F.J. Aoiz, M. Menendez, E. Verdasco, Phys. Chem. Chem. Phys. 2 (2000) 589.
[28] V. Piermarini, A. Laganà, G.G. Balint-Kurti, Phys. Chem. Chem. Phys. 3 (2001) 4515.
[29] H. Tal-Ezer, R. Kosloff, J. Chem. Phys. 81 (1984) 3967.
[30] F. Göğtas, G.G. Balint-Kurti, C.C. Marston, Quantum chemistry program exchange, program No. 647, QCPE Bull. 14 (1994) 19.

[31] J.C. Light, I.P. Hamilton, V.J. Lill, J. Phys. Chem. 82 (1985) 1400.
[32] W.H. Press, B.P. Flannery, S.A. Teukolsky, W.T. Vetterling, Numerical Recipes, Cambridge University Press, Cambridge, 1986, ISBN: 0 521 30811 9.
[33] R. Kosloff, J. Phys. Chem. 92 (1988) 2087.
[34] G.C. Schatz, A. Kuppermann, J. Chem. Phys. 65 (1976) 4642.
[35] M. Baer, in: M. Baer (Ed.), Theory of Chemical Reaction Dynamics, vol. 1, CRC Press, Boca Raton, FL, 1985, p. 91.
[36] Á. Vibó, G.G. Balint-Kurti, J. Chem. Phys. 96 (1992) 7615.
[37] Á. Vibók, G.G. Balint-Kurti, J. Phys. Chem. 96 (1992) 8712.